# Potential of Wollastonite-Based Brushite Cement for the Conditioning of Radioactive Waste Contaminated by $^{90}Sr$

Jihane Jdaini *, Céline Cau Dit Coumes, Yves Barré, Marie-Noëlle de Noirfontaine, Mireille Courtial

Posted Date: 5 February 2026

doi: 10.20944/preprints202602.0348.v1

Keywords: radioactive waste; strontium; cement; leaching; gamma irradiation

 doi:10.20944/preprints202602.0348.v1



*Article*

# Potential of Wollastonite-Based Brushite Cement for the Conditioning of Radioactive Waste Contaminated by $^{90}Sr$

**Jihane Jdaini [1,2,*], Céline Cau Dit Coumes [1], Yves Barré [3], Marie-Noëlle de Noirfontaine [2] and Mireille Courtial [2,4]**

1 CEA, DES, ISEC, DPME, SEME, Univ Montpellier, Marcoule, France
2 Laboratoire des Solides Irradiés, CEA, CNRS, Ecole Polytechnique, Institut Polytechnique de Paris, 91128 Palaiseau, France
3 CEA, DES, ISEC, DMRC, STDC, Univ Montpellier, Marcoule, France
4 Université d'Artois, 62408 Béthune, France
* Correspondence: jihane.jdaini@cea.fr

**Abstract**

This work investigates the potential of wollastonite-based brushite cement (WBC) for the stabilization and solidification of radioactive waste contaminated by $^{90}Sr$. This phosphate binder was formed by the reaction of wollastonite ($CaSiO_3$) with a phosphoric acid solution containing borax and metallic cations ($Al^{3+}$, $Zn^{2+}$). Two cement pastes were investigated: a commercial binder (WBC-C) and an optimized formulation (WBC-O), produced using a zinc-free mixing solution with a higher aluminum content than that of WBC-C. Both materials mainly contained amorphous hydrated silica and calcium aluminophosphate, along with crystalline brushite, residual wollastonite, and quartz. The stability of WBC-C under γ-irradiation was evaluated up to a dose of 1 MGy. The only observable effect was water radiolysis, leading to dihydrogen production at yields comparable to Portland cement matrices and geopolymers. Strontium leaching, assessed using the ANSI/ANS-16.1 procedure, followed a two-stage release mechanism combining surface wash-off and diffusion. The apparent diffusion coefficient $D_a$ of Sr in WBC-C was three orders of magnitude lower than typical values reported for Portland cement matrices. WBC-O showed enhanced Sr retention due to its higher aluminum content, which refines mesopores and reduces diffusion pathways accessible to Sr. WBC binders therefore appear to be promising candidates for strontium immobilization.

**Keywords:** radioactive waste; strontium; cement; leaching; gamma irradiation

## 1. Introduction

Aqueous radioactive waste, primarily contaminated with cesium and strontium, may be generated by cleaning operations carried out as part of the decommissioning of old nuclear facilities [1]. After a volume-reduction, typically involving evaporation, co-precipitation and filtration, or sorption onto ion exchange materials, the resulting low-level or intermediate-level radioactive waste is usually encapsulated in a cement-based matrix prior to disposal [2]. This conditioning step is intended to prevent waste dispersion, facilitate handling and transportation, and limit the release of hazardous elements that could endanger human health and the environment. Portland cement, possibly blended with supplementary cementitious materials such as blastfurnace slag or fly ash, is commonly used to design cement-based matrices [3]. This binder is indeed readily available, compatible with aqueous waste (as the water in the waste is used up for cement hydration), and generally exhibits good mechanical strength after hydration, long-term stability, and high alkalinity – favorable to the precipitation and confinement of many radionuclides, including actinides [3,4]. Nonetheless, its capacity to retain critical radionuclides, such as $^{137}Cs$ and $^{90}Sr$, may be limited [5–7].

 doi:10.20944/preprints202602.0348.v1



This study focuses on $^{90}Sr$, a high-energy β-emitter, that is particularly toxic due to its chemical similarity to calcium, which allows it to readily bind to bone tissues [8,9]. The aim of this work is to evaluate the potential of a calcium phosphate binder as an alternative to Portland cement for enhancing strontium retention. Calcium phosphate cements are used in dentistry and orthopedic bone filling surgeries since they form products with chemical compositions similar to those of bones and teeth [10–16]. In particular, wollastonite-based brushite cement (WBC) is a phosphate binder prepared by mixing wollastonite, a natural meta-silicate mineral ($CaSiO_3$), with a solution containing phosphoric acid, boron and metallic cations (such as $Al^{3+}$ and $Zn^{2+}$) [17–19]. Wollastonite reacts through dissolution/precipitation, resulting in a multiphase material that includes brushite ($CaHPO_4.2H_2O$), amorphous calcium aluminophosphate, amorphous silica, and residual wollastonite [17]. Brushite ($CaHPO_4.2H_2O$) is well-known for its flexible structure, allowing for the substitution of strontium in place of calcium [20–23]. Additionally, as compared to other phosphate binders, WBC offers the advantage of being cost-effective due to the raw materials used and the ability to prepare it at room temperature.

The retention properties of solidified cement matrices used for the immobilization of radioactive waste are commonly assessed through leaching tests. In a previous study [24] where leaching experiments were conducted according to the ANS/ANSI-16.1 standard [25], we showed that strontium retention was significantly improved when using a commercial WBC binder compared to conventional Portland cement. The apparent diffusion coefficient ($D_a$) of strontium in WBC paste was found to be approximately three orders of magnitude lower than values typically reported for Portland cement-based matrices. These findings highlight the strong potential of WBC-based materials for effective strontium encapsulation.

However, beyond radionuclides retention challenges, another concern for cement-based materials devoted to radioactive waste conditioning is the hydrogen gas production resulting from radiolysis of water – either present as free water in the pore solution, or chemically bound to the cement hydrates [26–30]. Gas accumulation in the cemented waste packages may induce pressure built-up, finally leading to cracking, which decreases their mechanical and confining properties [31,32]. Besides, hydrogen gas may form combustible or explosive mixtures with atmospheric oxygen when its concentration exceeds 4%, which raises a major safety issue for disposal facilities.

To fully assess the suitability of WBC-based materials for radioactive waste conditioning, it is important to investigate their behavior under ionizing radiation, as would occur in the presence of radionuclides within encapsulated waste. Although strontium is a 100% β-emitter, it may be conditioned with other radionuclides emitting $\alpha$ or $\beta\gamma$ radiations, which justifies focusing on γ-irradiation in this study. Accordingly, the first part of this work evaluates the response of a commercial WBC binder, along with its main crystalline hydrate, brushite, to external γ-irradiation using a $^{60}Co$ source. The total integrated dose (1 - 5 MGy) was representative of the dose that may be absorbed by a cement-waste form over its lifetime. The dihydrogen gas production was measured by gas chromatography, and possible structural damages in the solid phases were looked for using X-ray diffraction.

In addition to the behavior of WBC binders under irradiation, the influence of the formulation parameters on strontium retention also needs to be assessed, as the mineralogy of these binders depends on the composition of the mixing solution. Recent investigations by Laniesse *et al.* [18] examined how the concentrations of phosphoric acid, boron (added as borax or boric acid), and metallic cations (such as $Al^{3+}$ and $Zn^{2+}$) influence the setting time, mineralogy, and mechanical properties of WBC binders. Boron was found to delay the setting time of the cement paste and reduce its self-heating during hydration [18]. However, the resulting material exhibits poor mechanical properties. In contrast, metallic cations acted as setting accelerators. Specifically, zinc promoted the formation of scholzite ($CaZn_2(PO_4)_2 \cdot 2H_2O$), a crystalline calcium zinc phosphate, while aluminum led to the formation of an amorphous calcium aluminophosphate [18]. Increasing the aluminum concentration in the mixing solution significantly improved the mechanical strength of the hardened material. Building on these results, Laniesse *et al.* [18] identified an optimal composition range for the

 doi:10.20944/preprints202602.0348.v1



mixing solution ($[H_3PO_4]$ = 9 mol·L$^{-1}$, $[Al^{3+}]$ = 1.8 to 2.5 mol·L$^{-1}$, [B] = 0.2 to 0.6 mol·L$^{-1}$) that produces a material with suitable properties for waste conditioning, including a setting time between 4 and 48 hours, a compressive strength greater than 30 MPa, and a maximum heat flow below 5 mW/g.

While the effect of the mixing solution composition on the mineralogy and mechanical properties of WBC binders is well established, its influence on strontium retention remains unclear. To address this gap, the second part of this study investigates a WBC paste formulated with an optimized mixing solution ($[H_3PO_4]$ = 9 mol·L$^{-1}$, $[Al^{3+}]$ = 2.5 mol·L$^{-1}$, [B] = 0.2 mol·L$^{-1}$). Leaching tests, conducted in accordance with the ANS/ANSI-16.1 standard procedure [25], were used to quantify strontium release and to determine the corresponding apparent diffusion coefficient ($D_a$) and leachability index (LI). The results are compared with those previously obtained for a commercial WBC binder [24] and for conventional cement-based matrices.

## 2. Experimental

### *2.1. Materials and Samples Preparation*

To investigate the influence of WBC formulation on strontium retention, two cement pastes were studied in this work (**Table 1**). Both were prepared using the same commercial wollastonite powder ($CaSiO_3$, supplied by Sulitec), characterized by a specific surface area of 1.2 m$^2$·g$^{-1}$ and a particle size distribution of $d_{10}$ = 2.8 µm, $d_{50}$ = 15.2 µm, and $d_{90}$ = 48.3 µm. It was slightly carbonated, containing 2.1 ± 0.2 wt.% $CaCO_3$, as determined by thermogravimetry analysis (TGA), and contained trace amounts of quartz.

The first paste, referred to as WBC-C (Commercial formulation), was prepared using a commercial mixing solution (also provided by Sulitec), with the following composition: $[H_3PO_4]$ = 9.3 mol·L$^{-1}$, $[Al^{3+}]$ = 1.6 mol·L$^{-1}$, $[Zn^{2+}]$ = 1.5 mol·L$^{-1}$, and [B] = 0.6 mol·L$^{-1}$ (added as borax). The second paste, referred to as WBC-O (Optimized formulation), was prepared using a synthetic mixing solution based on optimized compositions reported in [18], containing $[H_3PO_4]$ = 9 mol·L$^{-1}$, $[Al^{3+}]$ = 2.5 mol·L$^{-1}$, and [B] = 0.2 mol·L$^{-1}$. Sr-doped WBC-C and Sr-doped WBC-O pastes were also prepared, as summarized in **Table 1**.

All pastes were prepared using a standardized mixer in accordance with European standard 196-1. The two components were mixed for 5 min at low speed, with a liquid-to-solid (L/S) weight ratio of 1.25, resulting in a Ca/P molar ratio also equal to 1.25. For leaching experiments, stable strontium was used as a surrogate for its radionuclide and was added to the mixing solution as $Sr(NO_3)_2$ (Merck, > 99% purity) at a concentration of $[Sr^{2+}]$ = 1 g·L$^{-1}$. Paste samples for leaching experiments were cast into polypropylene cylindrical containers (30 mL in volume) that were tightly sealed and cured for 28 d at room temperature. Those intended for irradiation tests were poured into 15 mL plastic centrifuge tubes ("SuperClear", provided by VWR) that were immediately sealed to prevent desiccation and stored during 28 days at room temperature.

**Table 1.** Formulation of the investigated WBC pastes.

| Sample code | Composition of the mixing solution | $[Sr^{2+}]$ in the mixing solution (mg·L$^{-1}$) | Mixing solution (g) | Wollastonite (g) |
|---|---|---|---|---|
| WBC-C | $[H_3PO_4]$ = 9.3 mol·L$^{-1}$<br>$[Al^{3+}]$ = 1.6 mol·L$^{-1}$<br>$[Zn^{2+}]$ = 1.5 mol·L$^{-1}$<br>[B] = 0.6 mol·L$^{-1}$ | - | 62.5 | 50 |
| WBC-O | $[H_3PO_4]$ = 9 mol·L$^{-1}$ | - | 62.5 | 50 |

 doi:10.20944/preprints202602.0348.v1



| | | | | |
|---|---|---|---|---|
| | $[Al^{3+}]$ = 2.5 mol·L$^{-1}$<br>[B] = 0.2 mol·L$^{-1}$ | | | |
| Sr-doped WBC-C | $[H_3PO_4]$ = 9.3 mol·L$^{-1}$<br>$[Al^{3+}]$ = 1.6 mol·L$^{-1}$<br>$[Zn^{2+}]$ = 1.5 mol·L$^{-1}$<br>[B] = 0.6 mol·L$^{-1}$ | 1000 | 62.5 | 50 |
| Sr-doped WBC-O | $[H_3PO_4]$ = 9 mol·L$^{-1}$<br>$[Al^{3+}]$ = 2.5 mol·L$^{-1}$<br>[B] = 0.2 mol·L$^{-1}$ | 1000 | 62.5 | 50 |

The WBC-C paste was used for both irradiation and leaching experiments.

Synthetic brushite ($CaHPO_4.2H_2O$) was used in some irradiation experiments. The brushite powder ($d_{10}$ = 3.0 µm, $d_{50}$ = 11.8 µm, $d_{90}$ = 27.8 µm, specific surface area = 1.4 ± 0.1 m$^2$.g$^{-1}$) was provided by Accros Organics. It contained 95.80 wt.% brushite, 2.05 wt.% monetite $CaHPO_4$ and 2.15 wt.% newberyite $MgHPO_4.3H_2O$, as determined in [33].

*2.3. Irradiation Experiments*

The WBC-C samples used for irradiation experiments consisted of small cylinders (15 mm in diameter, approximately 5.6 cm in height) containing 10 mL of cement paste and cured for 28 d in their airtight plastic tubes at room temperature. Prior to irradiation, the samples were demolded, weighed (~ 20 ± 2 g), introduced into 100 mL glass tubes, deaerated by applying 3 cycles of depressurization at 30 hPa and pressurization with argon, and finally flame-sealed under 900 hPa of pure argon (Alphagaz 1 of Air Liquide). A previous study showed that water loss due to desiccation during the sealing process was less than 1% of the total water content of the paste samples [34].

Irradiation experiments were also carried out on brushite powder. Samples of 1 ± 0.05 g were introduced in 100 mL glass tubes that were deaerated and sealed following the same protocol as for the cement pastes.

Gamma irradiations were performed in Steris Gammatec experimental irradiator located in Marcoule, France, and equipped with a $^{60}$Co source (energy of 1.2 MeV). The temperature of the irradiation chamber was regulated between 20 and 25°C and the dose rate was close to 1000 Gy.h$^{-1}$. The integrated doses were equal to 100 kGy, 250 kGy, 500 kGy and 1 MGy for the cement pastes, and to 250 kGy, 500 kGy, 750 kGy, 1 MGy, 2.5 MGy and 5 MGy for brushite powder. The experiments were conducted in triplicate for pastes and in duplicate for powders.

In a recent study, Herin *et al.* [35] showed that hydrogen gas release from portlandite exposed to accelerated electrons or gamma irradiation occurs almost instantaneously for $H_2$ formed near or at the surface of the crystals, but continues, at a slower rate, over a two-month period for $H_2$ trapped within the bulk of the material. Based on these observations, the authors thus recommended to heat the sample at 180°C for 3 days to fully release the stored hydrogen. However, this thermal treatment was unsuitable for our samples, as it would cause significant thermal decomposition of the cement hydrates (see Section 3.1). Instead, the glass tubes were stored for three weeks after irradiation to allow hydrogen to diffuse through the cementitious materials. Calculations using a $H_2$ diffusion coefficient of 5×10$^{-9}$ m$^2$.s$^{-1}$ (which is typical for a Portland-cement based material [36]) and taking into account the small size of the samples showed that gas accumulation within the paste was negligible after this 3-week period. Subsequently, the dihydrogen content present in the gas phase was

 doi:10.20944/preprints202602.0348.v1



determined by gas chromatography (Agilent 7820A), using argon as the carrier gas, a capillary column, and a thermal conductivity detector. The $H_2$ concentration (in $mol.kg^{-1}$) was given by equation (Eq. 1):

$$[H_2] = \frac{P.f(H_2).V_t}{R.T.m_{sample}} \quad \text{(Eq. 1)}$$

where $P$ (in Pa) is the gas pressure in the glass tube after irradiation, $f(H_2)$ the volume fraction of $H_2$ determined by gas chromatography, $V_t$ the volume of the glass tube (in $m^3$), $R$ (in $J.mol^{-1}.K^{-1}$) the ideal gas constant, $T$ (in K) the sample temperature and $m_{sample}$ (in kg) the sample mass. The radiolytic yield of hydrogen $G(H_2)_{material}$ (in $mol.J^{-1}$) was then given by the slope of the gas production versus absorbed dose $D$ (in Gy) plot (Eq. 2).

$$G(H_2)_{material} = \frac{[H_2]}{D} \quad \text{(Eq. 2)}$$

Therefore, $G(H_2)_{material}$ represented the amount of hydrogen produced by the material for 1 J of absorbed energy. The experimental error associated to the determination of $G(H_2)_{material}$ was close to 10% for radiolytic yields higher than $10^{-9}$ $mol.J^{-1}$, but increased up to 50% for smaller yield values.

Since water was the only significant source of hydrogen in the irradiated samples, the hydrogen radiolytic yield $G(H_2)_{material}$ was also standardized with respect to the total mass of water ($w_{water}$) present in the samples (Eq. 3):

$$G(H_2)_{water} = \frac{G(H_2)material}{w_{water}} \quad \text{(Eq. 3)}$$

This normalized radiolytic yield was useful to compare the $H_2$ production when the samples did not contain the same amount of water.

### 2.2. Leaching Experiments

Leaching experiments were conducted following a protocol derived from ANSI/ANS-16.1 specification. The test was performed at room temperature (22 ± 2°C) by immersing a cylindrical paste specimen with a diameter of 27.4 mm and a height of 16.2 mm for 90 d in ultrapure water as the leachant for 90 d. The leachate was refreshed with new water nine times over the course of 3 months (at 2 h, 7 h, 24 h, 48 h, 5 d, 7 d, 14 d, 45 d, 90 d) to limit the accumulation of dissolved species (**Figure 1**). The volume of the leachant was set to 2 cm per unit of external geometric surface area of the specimen, rather than the recommended 10 cm. This reduction in leachant volume increased the concentration of strontium in the leachates, making it easier to detect. A previous attempt with the 10 cm ratio resulted in Sr concentrations below the detection limit (1 ppb) of the analytical method used. However, this change in the protocol also led to more significant changes in the leachant composition between renewals. Strontium ions, as well as the major elements of the cement matrix (Ca, P, Si, Al and Zn) released in the leachates, were analyzed using inductively-coupled plasma atomic emission spectroscopy (ICP-AES, ThermoFisher iCAP 3600 duo).

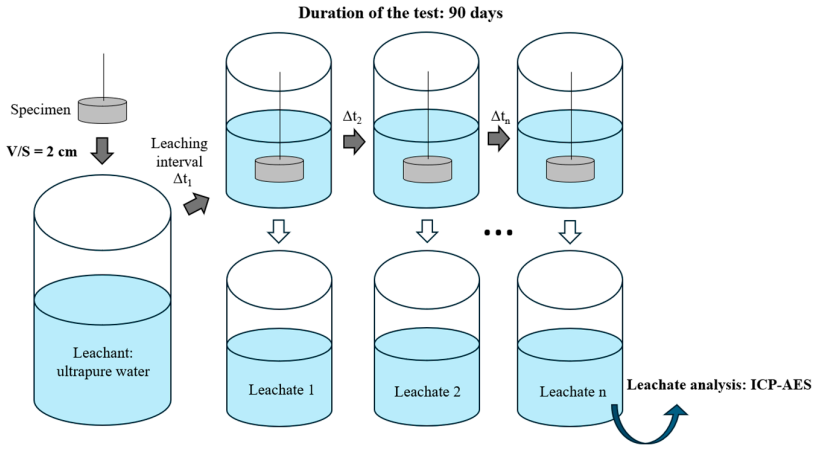


**Figure 1.** Leaching test procedure.

 doi:10.20944/preprints202602.0348.v1



The cumulative fraction of strontium leached (CFL) was calculated following Eq. 4.

$$CFL = \frac{\sum A_n}{A_0} \quad \text{(Eq. 4)}$$

where $A_n$ [g] is the amount of strontium released from the specimen during leaching interval n and $A_0$ [g] is its initial amount in the specimen.

### *2.4. Solid Phase Characterization*

#### 2.4.1. Hydration Stoppage

Before characterization, the pristine and irradiated cement pastes were submitted to hydration stoppage through solvent exchange with isopropanol following the procedure recommended by RILEM TC-238 SCM [37]. The residual isopropanol was then eliminated by gentle drying in a desiccator maintained at 20°C and 23% R.H. to prevent any thermal degradation of brushite [38].

#### 2.4.2. X-Ray Diffraction

The pristine and irradiated paste samples were characterized by X-ray diffraction (XRD) using a Panalytical X'Pert Pro diffractometer. First, the samples were finely ground by hand at a particle size below 80 µm. Since wollastonite crystallizes as fine needles [39], the paste samples were analysed using the Debye-Scherer configuration (transmission mode). They were introduced in Lindeman tubes (Φ = 0.7 mm) and mounted on a rotating goniometric head during measurement to minimize the preferred orientation effect. Silicon (Alfa Aesar 99.5% metal basis, ≈ 40 µm), was added to the samples as an internal standard (at a content of 10 wt.%) when the different phases were quantified with the Rietveld method [40]. The XRD data were recorded by using copper radiation ($\lambda_{CuK\alpha}$ = 1.5418 Å) at room temperature in the 2-θ range 5-70° with a step size of 0.013° for a total counting time of 2 h. Diffrac.EVA software (Bruker-AXS; V4.3, 2010-2018) and PDF-2 database (Powder Diffraction File, version 2009) were used for phase identification. Structural refinement of the XRD pattern of pristine cement paste was based on the crystallographic structures of brushite, wollastonite (triclinic) and quartz (impurity in wollastonite) respectively established by Schofield *et al*. [41], Ohashi [42] and Antao *et al*. [43]. It was carried out with TOPAS software (Bruker-AXS; V6, 2016) using the fundamental parameters approach and the ICSD database (ICSD files n° 172258, 201537 and 162490 for brushite, wollastonite and quartz, respectively). For all adjustments, the refined parameters were the phase scale factors, sample displacement, background modelled by a Chebyshev polynomial (order 5) combined with a 1/X term, unit cell and microstructural parameters. The atomic positions, site occupancies and temperature factors were kept constant during the refinement. Preferred orientation of brushite and wollastonite in the samples was taken into account using the March-Dollase correction [44].

Brushite samples were analyzed using a D8 Advance powder X-ray diffractometer (Bruker, Germany) with a copper radiation source in the Bragg-Brentano geometry (reflexion mode). The instrument was operated in step-scan mode, between 5° and 120° (2θ) with 0.007° (2θ) step and 1 s per step. An automatic anti-scattering knife was used to reduce unwanted scattered radiation by the atmosphere at low angles from the main beam. In order to minimize preferential orientation, the powders were prepared on Si wafers as zero-background holders to improve the detection of a potential diffusion halo. The Rietveld refinements of brushite samples were performed following the method previously described.

#### 2.4.3. Thermogravimetry

To determine the water content of cement pastes and brushite submitted to irradiation, thermogravimetric analyses (TGA) were carried out on ground samples using a TGA/DSC Netzsch STA 409 PC instrument operating under nitrogen (gas flow set at 50 mL.min$^{-1}$) at 10°C.min$^{-1}$ up to 1000°C. The curves were corrected from buoyancy effects by performing a blank subtraction.

 doi:10.20944/preprints202602.0348.v1



2.4.4. X-Ray Fluorescence

X-ray fluorescence (XRF) measurements were carried out on the solid fraction of the pristine cement paste to determine its chemical composition. The ground powder was fused at 950°C with a sample-to-lithium metaborate ratio equal to 0.05. The pellet was then analyzed using a Bruker XRF instrument (S8 Tiger).

2.4.5. Porosity

Total porosity accessible to water of 28 d–old WBC pastes was determined following NF P 18-459 (2010). Three cylindrical paste samples (≈15 g per sample) were placed in a vacuum desiccator at 25 mbar for 4 h. Then, samples were covered with demineralized water while maintaining the vacuum pressure at 25 mbar for a minimum of 44 h. After the immersion period, suspended and saturated weights of samples were determined. Finally, samples were dried to a constant weight in an oven at 75°C to preserve the integrity of brushite, which is unstable at higher temperatures [38,45]. Pore size distribution was determined using Mercury Intrusion Porosimetry (MIP) with an AutoPore IV 9500 Porosimeter from Micromeritics Instrument Corporation, following ISO 15901-1 (2005) standard. MIP analyses were performed on small pieces of paste of approximately 1–3 g, after hydration stoppage and drying, as described in section 2.4.1. The mercury pressure varied from 0.0014 MPa to 400 MPa, and the pore entry size diameters were > 3 nm.

## 3. Results and Discussion

*3.1. Characterization of Pristine WBC Paste Samples*

The pristine WBC-C and WBC-O paste samples exhibited very similar diffraction patterns after 28 days of curing under endogenous conditions (**Figure 2**). Both materials contained brushite ($CaHPO_4{\cdot}2H_2O$) and residual wollastonite ($CaSiO_3$). Quartz, an impurity present in the wollastonite powder, was also evidenced. The corresponding Sr-doped pastes (Sr-doped WBC-C and Sr-doped WBC-O), displayed identical mineralogical features. No new crystalline phase related to the addition of strontium in the cement matrices was detected.

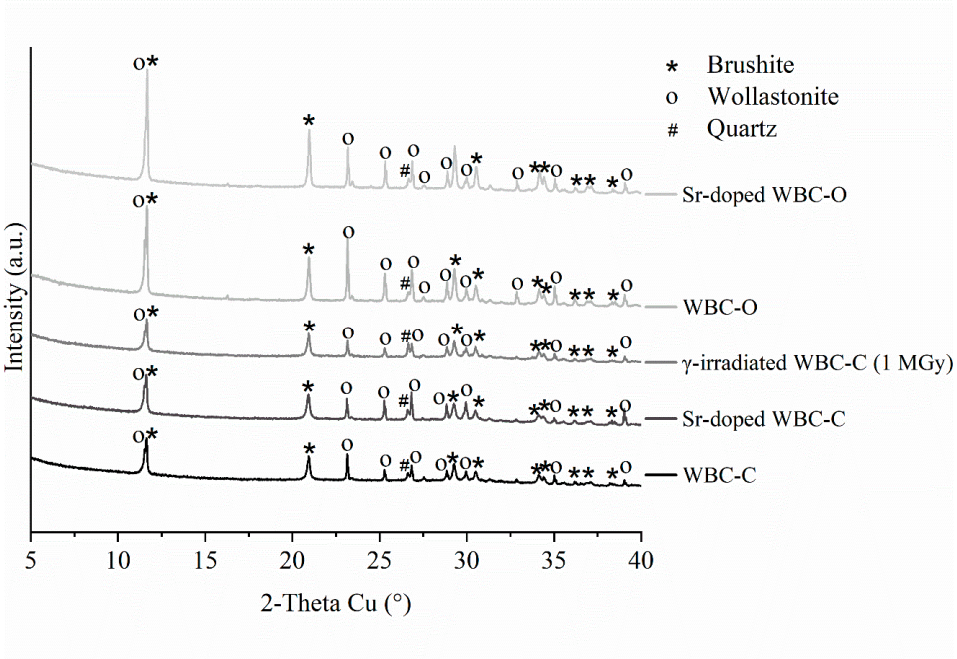


**Figure 2.** X-ray diffraction patterns of WBC-C, WBC-O, Sr-doped WBC-C, Sr-doped WBC-O and γ-irradiated (1 MGy) WBC-C pastes.

 doi:10.20944/preprints202602.0348.v1



The weight fractions of each crystalline phase and of total amorphous were determined by Rietveld refinement. The results are presented hereafter for reference WBC-C and WBC-O pastes, but were very similar for Sr-doped samples due to their very low Sr content (0.09% of $Sr(NO_3)_2$). To calculate the mass of each phase at 28 d, it was first necessary to determine the mass of the solid fraction. This latter could not be simply obtained by adding the bound water content determined by TGA to the initial mass of cement since the reactions occurring during hydration not only consumed water, but also ions from the mixing solution (phosphate, aluminum, zinc, boron, sodium). A previous study showed that the pore solution contained very low concentrations of silicate (less than 2 $mmol.L^{-1}$), regardless of the characterization time [18]. As a first approximation, dissolved silica could therefore be neglected, and silicon was considered to be present only in the solid phase, in the form of amorphous silica, wollastonite and quartz. According to mass conservation equation (Eq. 5), the total mass of silicon in the solid phase at 28 d ($m_{Si}^{solid}$) was thus assumed to be equal to the initial mass of silicon introduced via wollastonite and quartz.

$$m_{Si}^{solid} \approx m_{Si}^{init} \quad \text{(Eq. 5)}$$

The mass of solid at 28 d ($m^{solid}$) was then derived from Eq. 6:

$$m^{solid} = \frac{m_{Si}^{solid}}{f_{Si}^{solid}} \approx \frac{m_{Si}^{init}}{f_{Si}^{solid}} \quad \text{(Eq. 6)}$$

with $f_{Si}^{solid}$ the weight fraction of Si in the solid.

This latter was determined by XRF (**Table 2**). Then, knowing the mass of solid at 28 d, the mass of each crystalline phase was calculated using the Rietveld refinement results. The mass of amorphous silica ($m_{SiO_2 \cdot 3.93H_2O}$) was derived from mass balance equation (Eq. 7), considering $SiO_2 \bullet 3.93H_2O$ stoichiometry established experimentally by Jdaini [46] in a 28 d-old WBC paste prepared with a mixing solution containing $H_3PO_4$ (9 $mol.L^{-1}$) and borax (0.05 $mol.L^{-1}$). Finally, the Ca/P, Zn/P and Al/P molar ratios in the amorphous phase were calculated using mass conservation (**Table 2**).

$$m_{SiO_2 \cdot 3.93H_2O} = \left(m_{SiO_2}^{init} - m_{CaSiO_3} \times \frac{M_{SiO_2}}{M_{CaSiO_3}}\right)\left(1 + 3.93 \times \frac{M_{H_2O}}{M_{SiO_2}}\right) \quad \text{(Eq. 7)}$$

with $m_{CaSiO_3}$ the mass of wollastonite at 28 d, $M_{SiO_2}$, $M_{CaSiO_3}$ and $M_{H_2O}$ the molar weights of silica, wollastonite and water respectively.

**Table 2. Chemical and mineralogical compositions of pristine 28 d-old WBC-C and WBC-O cement pastes.**

| XRF analysis | WBC-C (wt.%) | WBC-O (wt.%) | Phase composition | WBC-C (g/100 g of wollastonite) | WBC-O (g/100 g of wollastonite) |
|---|---|---|---|---|---|
| Ca | 17.9 | 17.2 | Brushite $CaHPO_4.2H_2O$ | 14.9 ± 2.2 | 41.2 ± 6.1 |
| Si | 13.4 | 13.3 | Wollastonite $CaSiO_3$ | 8.5 ± 1.2 | 22.1 ± 3.3 |
| P | 11.6 | 11.3 | Quartz $SiO_2$ | 2.5 ± 0.4 | 3.6 ± 0.6 |
| Zn | 3.69 | - | Amorphous silica $SiO_2.3.93H_2O$ | 97.9 ± 14.6 | 81.8 ± 12.2 |
| Al | 1.4 | 2.65 | Amorphous aluminophosphate | 56.9 ± 8.5 *Ca/P = 1.1 ± 0.1 Al/P = 0.16 ± 0.02 Zn/P = 0.17 ± 0.02* | 36.1 ± 5.4 *Ca/P = 0.84 ± 0.1 Al/P = 0.42 ± 0.1* - |
| Na | 0.902 | - | Pore solution | 44.4 ± 6.6 | 39.7 ± 5.9 |
| Mg | 0.392 | 0.352 | | | |
| Fe | 0.214 | 0.189 | | | |

 doi:10.20944/preprints202602.0348.v1



**Mineralogical composition of pristine 28°d-old WBC-C and WBC-O pastes (wt.%)**

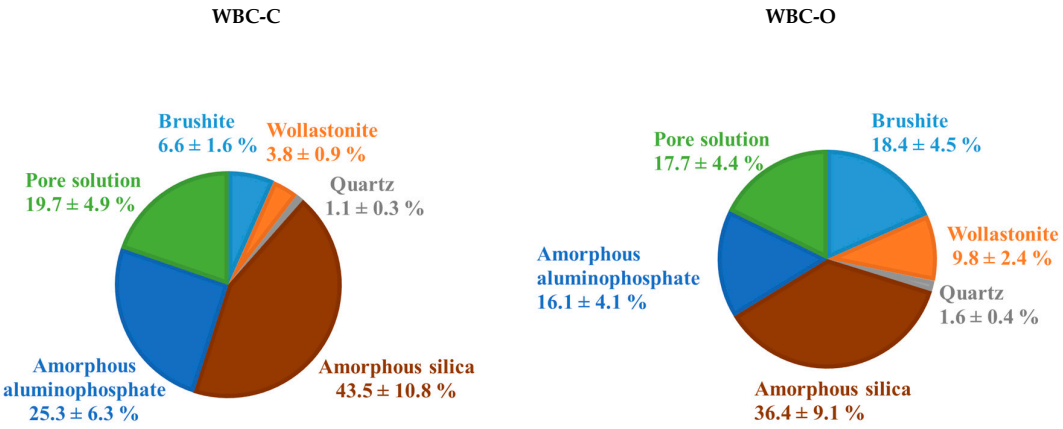


The concentration of boron in the solid fraction of the cement paste could not be determined since lithium metaborate was used as a reagent for alkaline fusion. Its contribution to the mass balance was neglected in the calculations. However, it is worth noting that the mass fraction of boron in the cement pastes remained very low (0.54% for WBC-C and 0.18% for WBC-O).

Although referred as "brushite" cements, both pristine WBC-C and WBC-O paste samples were primarily composed of amorphous phases (aluminophosphate and hydrated silica). Brushite represented only 6.6 ± 1.6 wt.% of the 28 d-old WBC-C (including the pore solution), and 18.5± 4.5 wt.% of the 28 d-old WBC-O. The lower brushite content in WBC-C was consistent with the presence of zinc in the formulation, which is known to inhibit brushite formation [47]. The Zn/P and Al/P molar ratios of the aluminophosphate phase in WBC-C were consistent with those determined by Laniesse [47] on a similar material by SEM/EDX analyses (Zn/P = 0.15 ± 0.02, Al/P = 0.20 ± 0.02). A discrepancy was noticed concerning the Ca/P ratio (1.1 ± 0.1 in this study *vs.* 0.7 ± 0.05 in [47]). Nevertheless, Laniesse reported Ca/P values of 0.9 ± 0.1 for paste samples aged of 90 d, 180 d and 360 d, in better agreement with our finding.

WBC-O contained a higher amount of unreacted (residual) wollastonite (9.8 ± 2.4 wt.%) than WBC-C (3.8 ± 0.9 wt.%). This trend was also reported by Laniesse [47], who observed that increasing the initial aluminum concentration in the mixing solution resulted in a higher residual wollastonite content at 28 days. This effect can be attributed to the preparation protocol: aluminum is introduced as a metallic powder, which reacts with protons ($Al + 3\ H^+ \rightarrow Al^{3+} + 3/2\ H_2$) in the mixing solution. As more aluminum is added, the acidity decreases, which in turn slows down the dissolution of wollastonite.

Despite its lower initial aluminum content, WBC-C contained a larger fraction of amorphous aluminophosphate than WBC-O. This finding, also reported by Laniesse [47], may be related to the presence of zinc in WBC-C, which is absent in WBC-O. As previously discussed, $Zn^{2+}$ is known to inhibit brushite crystallization [47], potentially promoting the formation of amorphous aluminophosphate instead. The Ca/P and Al/P molar ratios of the aluminophosphate phase in WBC-O were 0.84 ± 0.1 and 0.42 ± 0.1 respectively, consistent with values reported by Laniesse for similar WBC formulations [47].

The thermograms and first derivatives of the pristine 28 d-old WBC-C and WBC-O paste samples are presented in **Figure 3**. For both materials, mass losses mainly occurred in three temperature ranges. In the 30°C – 170°C range, several thermal processes overlapped, including the evaporation of residual isopropanol (used for hydration stoppage) and physisorbed water, as well as the dehydration of amorphous silica (which occurs in the 45-100°C and 135°C-150°C intervals [48]) and aluminophosphate [18]. The weight loss observed between 170 and 220°C was mainly attributed to brushite dehydration [38,45]. A further weight loss between 400°C and 470°C resulted from the

 doi:10.20944/preprints202602.0348.v1



dehydroxylation and condensation of monetite ($CaHPO_4$) to form calcium pyrophosphate ($Ca_2P_2O_7$) [38]. Because this process did not overlap with other decomposition reactions, it was used to estimate the brushite content in the solid fraction of WBC-C and WBC-O pastes. The calculated values (12.8 ± 2.0 wt.% for WBC-C and 20.7 ± 2.7 wt.% for WBC-O) were in reasonable agreement with those derived from Rietveld refinement (8.2 ± 2.1 wt.% for WBC-C and 22.3 ± 5.6 wt.% for WBC-O). Both methods (TGA and XRD) consistently indicate a higher brushite content in the zinc-free WBC-O cement paste compared to WBC-C.

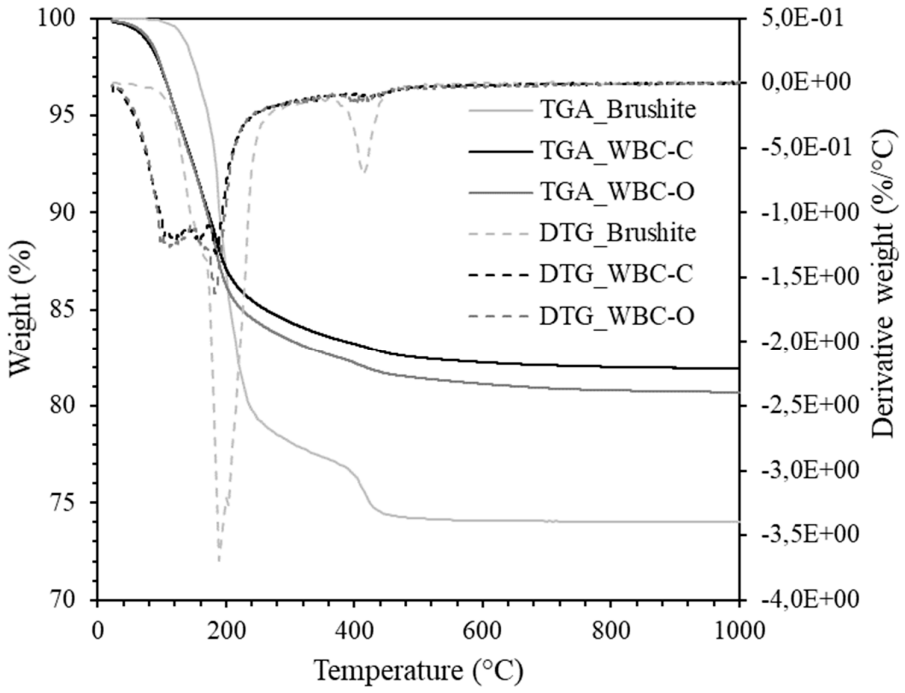


**Figure 3.** Thermograms of pristine WBC-C and WBC-O cement pastes and of pure brushite.

After 28 d of curing, WBC-C paste exhibited a total porosity accessible to water of 27.3 ± 0.7%, in good agreement with the total porosity accessible to mercury (28%). For comparison, Frizon *et al*. [36] reported a similar total porosity of 27% for a Portland cement paste with a water-to-cement (w/c) ratio of 0.35. The distribution of pore entry diameters (**Figure 4**) revealed that WBC-C paste presented two main modes centred at 0.012 µm and 0.3 µm, as well as a few macropores (mode at 600 µm) due to air entrapment, but also to the decarbonation of wollastonite in contact with the acidic mixing solution, which released carbon dioxide. In contrast, the WBC-O paste displayed its main pore size modes at finer diameters, around 0.005 µm and 0.08 µm. This refinement is consistent with the expected influence of aluminum on the pore structure. Laniesse *et al*. [18] showed that aluminum strongly influences the average diameter of mesopores: the higher its concentration, the smaller the pores. The average mesopore diameter of WBC-C (~107 Å at 90 d and ~80 Å at 180 d) was much larger than the values reported for WBC-O cement paste (~40 Å at 28 days) [18].

The porosity of WBC-C paste was less refined than that of a Portland cement paste at w/c = 0.35, where the peaks corresponding to capillary porosity and hydrate porosity were centred at 0.15 µm and 0.003 µm respectively [36].

 doi:10.20944/preprints202602.0348.v1



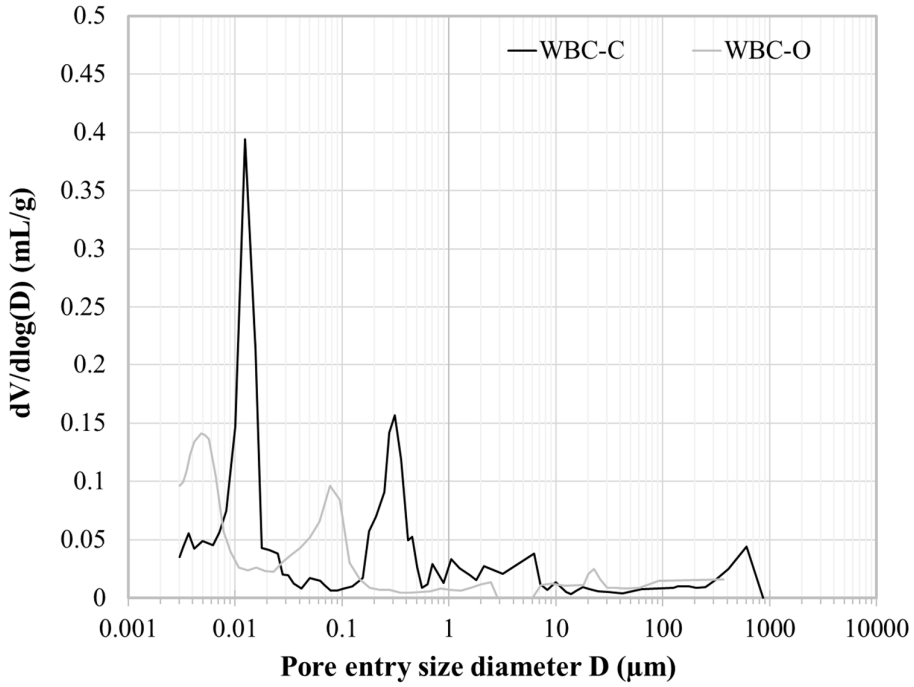


**Figure 4.** Pore entry size distributions of 28 d-old pristine WBC-C and WBC-O pastes obtained by MIP.

*3.2. Gamma Irradiation of WBC-C Paste*

3.2.1. Hydrogen Gas Production

28 d-old WBC-C paste samples, as well as brushite, their main crystalline hydrate, were submitted to external gamma irradiation. **Figure 5** plots the concentration of hydrogen gas released in the glass ampoules, normalized with respect to the weight of material, as a function of the integrated dose. In both cases, this concentration increased almost linearly up to 500 kGy, but tended to level off at higher doses, likely due to a recycling effect [27].

The radiolytic yields, $G(H_2)_{material}$, were given by the slopes of the regression lines in the 0 - 500 kGy dose range (Eq. 2) (**Table 3** and **Table 4**). The yields were also normalized with respect to the total mass of water present in the materials following (Eq. 3).

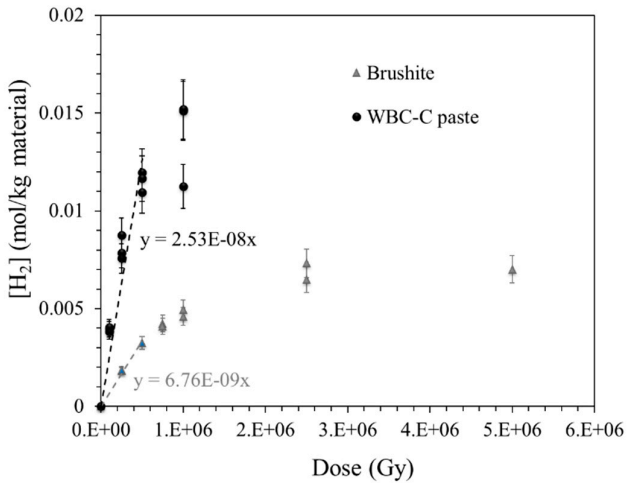


**Figure 5.** $H_2$ production by WBC-C paste and brushite as a function of the integrated dose (γ - irradiation).

 doi:10.20944/preprints202602.0348.v1



The $H_2$ radiolytic yields measured for WBC paste were of the same order of magnitude as those reported for geopolymer [49], Portland [29,50] or calcium sulfoaluminate [29] cement pastes. In comparison, calcium aluminate and magnesium phosphate cement pastes had significantly lower yields [30,34]. It can be noted that $G(H_2)_{water}$ measured for WBC-C paste ($1.10 \pm 0.11 \times 10^{-7}$ mol/J) was about three times higher than that reported for free water ($0.44 \pm 0.04 \times 10^{-7}$ mol/J [51]) (**Table 3**).

**Table 3.** Comparison of $H_2$ radiolytic yields for different cement pastes (γ-rays).

| Type of paste | Mass fraction of water (%) | Dose | $G(H_2)_{material}$ $\times 10^{-7}$ (mol.J$^{-1}$) | $G(H_2)_{water}$ $\times 10^{-7}$ (mol.J$^{-1}$) | Ref. |
|---|---|---|---|---|---|
| WBC-C | 23.0 | 100 kGy up to 1 MGy | 0.25 ± 0.02 | 1.10 ± 0.11 | This work |
| Geopolymer Geo Na | 33.0 | 100 and 250 kGy | 0.13 ± 0.10 | 0.4 ± 0.04 | [49] |
| Geo K | 33.9 | | 0.25 ± 0.02 | 0.75 ± 0.07 | |
| Geo Cs | 26.8 | | 0.48 ± 0.04 | 1.80 ± 0.18 | |
| Portland cement | 16.7 37.5 | 1 MGy | 0.13 ± 0.10<br>0.33 ± 0.03 | | [50] |
| Portland cement (CEM I 52.5 N SR0 CE PM-CP2 NF) | 16.7 | 500 kGy | 0.05 ± 0.01 | 0.31 ± 0.03 | [30] |
| | 23.1 | | 0.07 ± 0.01 | 0.30 ± 0.04 | |
| | 28.6 | | 0.10 ± 0.01 | 0.32 ± 0.03 | |
| | 33.3 | | 0.11 ± 0.01 | 0.32 ± 0.03 | |
| | 37.5 | | 0.11 ± 0.01 | 0.30 ± 0.03 | |
| Calcium sulfoaluminate cement (85% clinker + 15% $CaSO_4$) | 28.6 | 100 and 200 kGy | 0.10 ± 0.01 | 0.37 ± 0.01 | |
| Calcium aluminate cement | 16.6 | 500 kGy | 0.009 ± 0.005 | 0.055 ± 0.005 | [30] |
| | 23.0 | | 0.018 ± 0.002 | 0.078 ± 0.008 | |
| | 28.4 | | 0.032 ± 0.003 | 0.11 ± 0.01 | |
| | 33.1 | 150 and 300 kGy | 0.057 ± 0.006 | 0.17 ± 0.01 | |
| | 37.3 | | 0.083 ± 0.008 | 0.22 ± 0.02 | |
| Magnesium phosphate cement (molar ratios) $MgO/KH_2PO_4 = 1$ $H_2O/MgO = 5$ | 40.5 | 150 and 300 kGy | 0.084 ± 0.010 | 0.21 ± 0.03 | [34] |
| Bulk water (pH 13) | | | | 0.44 ± 0.04 | [51] |

This could originate from the chemical composition of the pore solution, which contained a large panel of dissolved species (Al, Ca, P, Zn, B, Na) and a pH close to 6 [18]. Confinement of water within the cement matrix could also promote recombination of reductive species, leading to the formation of $H_2$, and / or an efficient energy transfer from the material to the neighboring -OH groups. Similar results were observed by Chupin on geopolymers [49], and were also reported in the case of C-S-H (**Table 4)** [52].

 doi:10.20944/preprints202602.0348.v1



**Table 4.** Comparison of $H_2$ radiolytic yields for different cement hydrates (γ-rays).

| Cement hydrate | Dose | $G(H_2)_{material}$ $\times 10^{-7}$ (mol.J$^{-1}$) | $G(H_2)_{water}$ $\times 10^{-7}$ (mol.J$^{-1}$) | Ref. |
|---|---|---|---|---|
| Brushite $CaHPO_4.2H_2O$ | 250 kGy up to 5 MGy | 0.070 ± 0.007 | 0.26 ± 0.02 | This work |
| Gibbsite $Al(OH)_3$ | 200 kGy | 0.009 ± 0.005 | 0.027 ± 0.003 | [30] |
| Katoite $Ca_3Al_2(OH)_{12}$ | 200 kGy | 0.003 ± 0.002 | 0.011 ± 0.001 | |
| Calcium monocarboaluminate hydrate $Ca_4Al_2(CO_3)(OH)_{12}.5H_2O$ | 200 kGy | 0.12 ± 0.01 | 0.38 ± 0.04 | |
| Portlandite $Ca(OH)_2$ | | 0.21 | | [53] |
| | 200 kGy | 0.042 ± 0.004 | 0.19 ± 0.03 | [54] |
| | 150 kGy | 0.081 ± 0.005 | 0.33 ± 0.02 | [35] |
| Brucite $Mg(OH)_2$ | 200 kGy | 0.055 ± 0.006 | 0.18 ± 0.03 | [54] |
| | | 0.053 | | [53] |
| Calcium Silicate Hydrate (C-S-H) with $CaO/SiO_2$ of: | | | | |
| 0.80 | 100 and 200 kGy | 0.61 ± 0.06 | 3.23 ± 0.32 | [52] |
| 0.97 | | 0.58 ± 0.06 | 3.11 ± 0.31 | |
| 1.14 | | 0.49 ± 0.05 | 2.85 ± 0.29 | |
| 1.30 | | 0.42 ± 0.04 | 2.44 ± 0.24 | |
| 1.40 | | 0.36 ± 0.04 | 2.13 ± 0.21 | |
| Bulk water (pH 13) | | 0.44 ± 0.04 | | [51] |

The $H_2$ radiolytic yield of brushite ($CaHPO_4.2H_2O$) given in **Table 4** should be considered as indicative. Indeed, two main uncertainties were associated to its determination. *(i)* The sample was not dried before irradiation. Thus, uncontrolled sorption of water could lead to overestimate the $H_2$ production. *(ii)* The brushite sample purity was 95.8% only. Nevertheless, the $G(H_2)$ value was of the same order of magnitude as those reported for portlandite, brucite and calcium monocarboaluminate hydrate (**Table 4**), but significantly higher than those reported for gibbsite and katoite, the two main hydrates of calcium aluminate cement that are known to exhibit good stability under irradiation [30].

If we assume, like Acher *et al.* [30], that the $H_2$ production yield of WBC paste is the sum of the yields of its hydrates and of free pore water, brushite, which accounts for 6.6 wt.% of the paste sample, would only contribute to 1.85% of the $H_2$ production. This suggests that water present in the amorphous hydrates and/or in the pore solution would be more prone to decompose into hydrogen gas under irradiation.

### 3.2.2. Mineralogy of Irradiated Materials

The mineralogy of WBC-C paste was characterized by XRD after irradiation at a dose of 1 MGy (**Figure 2**). Its X-ray diffraction pattern was very similar to that of the virgin sample. Both materials contained brushite, residual wollastonite and quartz. No new crystalline or amorphous phase that could produce a halo in the XRD pattern were observed. Moreover, the diffraction peaks did not show any broadening that could indicate the creation of defects in the crystalline phases induced by

 doi:10.20944/preprints202602.0348.v1



gamma irradiation. This was confirmed by investigating more specifically brushite, the main crystalline hydrate, after irradiation at doses ranging from 250 kGy to 5 MGy (**Figure 6**). No peak broadening was observed, nor the formation of new phases under irradiation. The crystal cell parameters of brushite were obtained from Rietveld refinement of the XRD patterns and showed no significant evolution with the integrated dose (**Figure 7**). The maximum relative volume change, $\Delta V/V$ = +0.073%, achieved by the unit cell of brushite under gamma irradiation (~ 1.2 MeV) at a dose of 5 MGy was approximately 3.57 times lower than the maximum expansion experienced by brushite under electron irradiation (2.5 MeV) at a much higher dose of 270 MGy, $\Delta V/V$ = +0.246% [55]. Amorphization of brushite into amorphous calcium pyrophosphate, which was observed under electron irradiation at doses higher than 270 MGy [33], was not observed in this study: the crystalline structure of brushite remained stable under gamma irradiation up to 5 MGy. Thus, WBC paste showed good stability under gamma irradiation in a range of doses relevant for LL- IL waste conditioning.

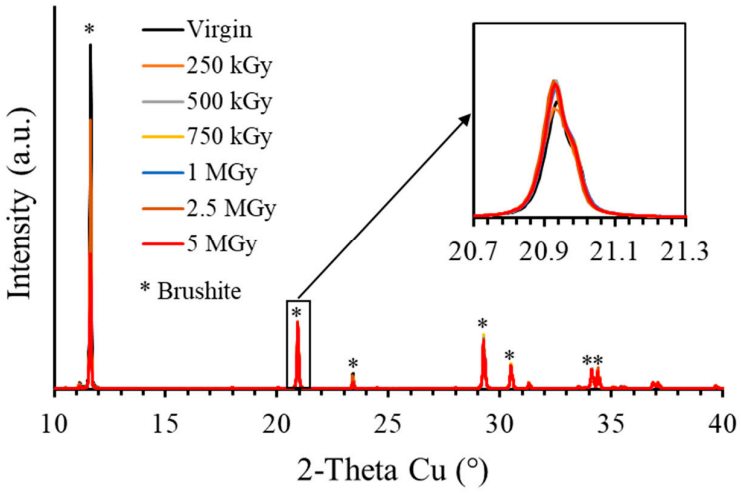


**Figure 6.** XRD patterns of virgin and γ-irradiated brushite samples.

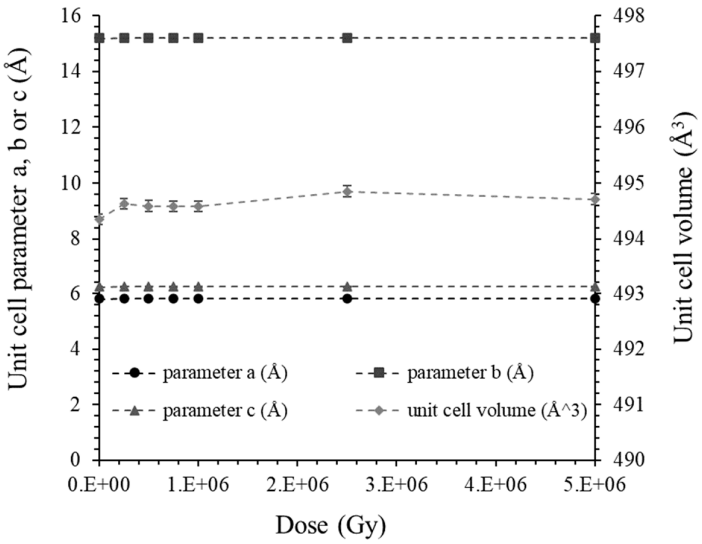


**Figure 7.** Evolution of unit cell parameters (a, b and c) and volume of virgin and γ-irradiated brushite samples as a function of the irradiation dose.

 doi:10.20944/preprints202602.0348.v1



*3.3. Leaching of Sr-Doped WBC Pastes*

3.3.1. Characterization of the Leachates

Leaching of Sr-doped WBC-C and WBC-O paste samples led to a release of Ca, Si, P and Sr into solution. This release was rapid in the first few days, and then gradually slowed down (**Figure 8**). Overall, slightly lower concentrations were measured for WBC-O compared to WBC-C, suggesting improved element retention in the optimized formulation. For both materials, the leached concentration of Sr was more than three orders of magnitude lower than those of Ca, Si and P. The Al and Zn concentrations always remained below the detection limit, indicating that the amorphous aluminophosphate phase exhibited better chemical durability than brushite under the investigated leaching conditions. The pH of the leachates, that was measured after each renewal, showed limited change over the test period, remaining within the range 6.5 - 7.5 (**Figure 8**).

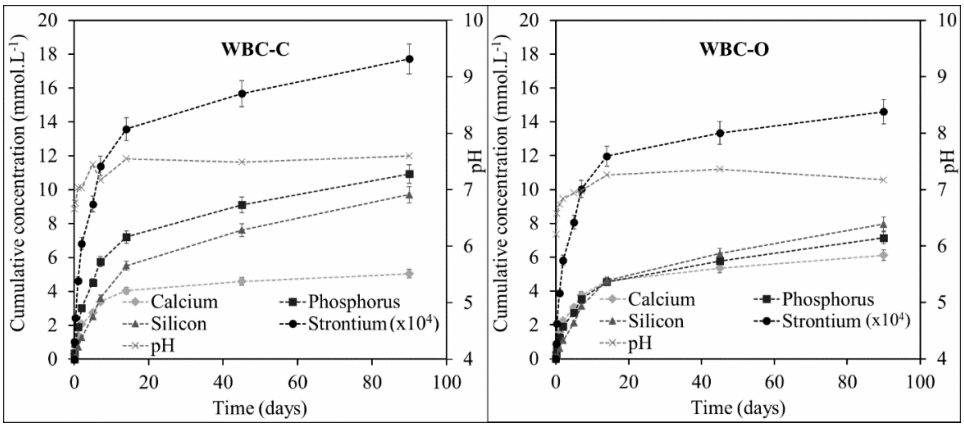


**Figure 8.** Evolution with time of pH and cumulative concentrations of Ca, P, Si and Sr ([Sr]×10⁴) released in the leachates for WBC-C (data from [24]) (left) and WBC-O (right) paste samples.

The evolution of the [P]/[Ca] concentration ratio in the leachates reveals distinct behaviors between the two cement pastes (**Figure 9**). For WBC-O, the ratio remained close to 1 throughout the test, suggesting a congruent dissolution of brushite ($CaHPO_4{\cdot}2H_2O$). In contrast, WBC-C exhibited a progressive increase in the [P]/[Ca] ratio, that reached values close to 2 by the end of the test. This trend aligns with previous XRD results reported for the same material [24], which showed the precipitation of calcium-deficient hydroxyapatite (CDHA), $Ca_9(HPO_4)(PO_4)_5(OH)$, on the exposed surface of leached WBC-C paste sample.

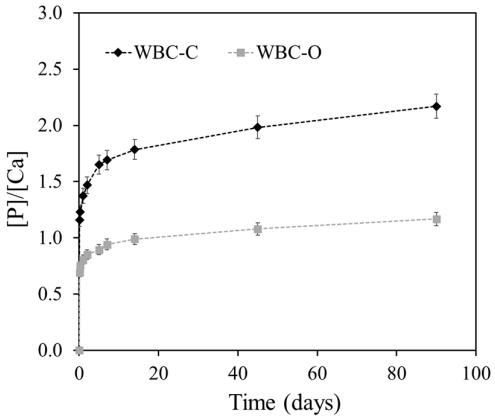


**Figure 9.** Evolution of the [P]/[Ca] concentration ratio in the leachates with time for Sr-doped WBC-C and Sr-doped WBC-O paste samples.

 doi:10.20944/preprints202602.0348.v1



The cumulative fractions of strontium leached (CFL) from both Sr-doped WBC pastes over 90 d are presented in **Figure 10**. At the end of the test, CFL values reached (1.22 ± 0.06)×10$^{-3}$ for WBC-C and (9.96 ± 0.49)×10$^{-4}$ for WBC-O, corresponding to the leaching of approximately 0.12% and 0.10% of the initial Sr content in the paste samples, respectively. These results indicate slightly improved Sr retention in WBC-O compared to WBC-C. The obtained CFL values are more than one order of magnitude lower than the data reported for Portland cement paste, which exhibits a CFL of around 5×10$^{-2}$ at w/c = 0.5 [56].

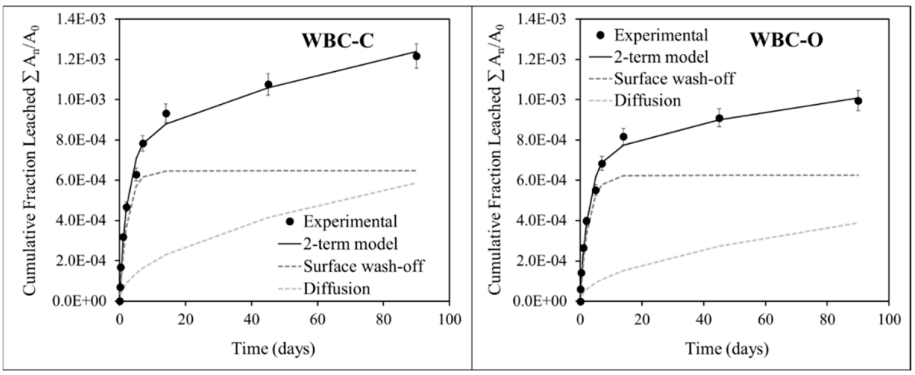


**Figure 10.** Experimental and calculated cumulative fractions of strontium leached from Sr-doped WBC-C (data from [24]) (left) and Sr-doped WBC (right) pastes. Use of a 2-term model taking into account surface wash-off and diffusion in the pore solution.

### 3.3.2. Modelling the Leaching of Strontium from WBC Pastes: Evaluation of the Diffusion Coefficient and Leachability Index

According to the literature, leaching from cementitious materials typically occurs via three main processes: surface exchange phenomena, diffusion of dissolved species in the pore network, and matrix dissolution [57,58]. Côté *et al.* [57] proposed a semi-empirical kinetic model that accounts for these mechanisms, incorporating contributions from surface wash-off (representing the "initial fraction leached"), diffusion and dissolution. The cumulative fraction leached (CFL) is described as a function of time using equation (Eq. 8).

$$CFL\ (t) = \frac{\sum A_n}{A_0} = k_1(1 - e^{-k_2 t}) + k_3 t^{1/2} + k_4 t \quad \text{(Eq. 8)}$$

To identify the dominant mechanisms controlling strontium leaching from WBC pastes, regression analysis was performed on the experimental CFL data using Eq. 8. Note that several assumptions were made to derive the leaching models leading to Eq. 8.

1. Time-invariant chemical environment: The leaching solution was periodically renewed to prevent accumulation of released species, and the pH remained relatively stable throughout the test.

2. Semi-infinite solid geometry: As defined by the ANS/ANSI 16.1 specification, the semi-infinite assumption is valid if the cumulative fraction leached is less than 20%. In this study, the cumulative fraction of strontium leached remained well below this threshold (~ 0.12% for WBC-C and 0.10% for WBC-O at the end of the test).

3. Zero surface concentration of strontium: The Sr concentrations in the leachates were consistently low (< 20 ppb), and the frequency of leachant renewal was high enough to support the boundary condition of zero surface concentration.

As a first approach, these assumptions were thus considered reasonably satisfied.

The optimized values of the model parameters are presented in **Table 5** and **table 6** for Sr-doped WBC-C and Sr-doped WBC-O pastes, respectively. In both cases, model showed excellent agreement with the experimental data, with adjusted $r^2$ values of 0.992 for WBC-C and 0.991 for WBC-O. Notably, parameter $k_4$ associated with matrix dissolution, was not statistically different from zero at a 95% confidence level for either material. This means that leaching was governed primarily by surface wash-off and diffusion. As a result, the model was simplified by omitting the third term in

 doi:10.20944/preprints202602.0348.v1



Eq. 8 and parameters $k_1$, $k_2$ and $k_3$ were recalculated. **Figure 10** compares the regression lines with the experimental CFL data for both paste samples. As expected, surface wash-off dominated during initial phase (day 1), followed by diffusion-controlled leaching over the remainder of the test.

**Table 5.** Coefficients from the regression analysis of CFL data for Sr-doped WBC-C paste [experimental data from [24]].

| Model | | Value | Standard Error | t-Value | Prob > \|t\| (%) |
|---|---|---|---|---|---|
| $CFL\ (t) = k_1(1 - e^{-k_2 t}) + k_3 t^{1/2} + k_4 t$ | $k_1$ | $4.04\times10^{-4}$ | $1.17\times10^{-4}$ | 3.45 | * |
| | $k_2$ | $4.92\times10^{-1}$ | $1.25\times10^{-1}$ | 3.93 | ** |
| | $k_3$ | $1.59\times10^{-4}$ | $4.50\times10^{-5}$ | 3.54 | * |
| $r^2_{adjusted} = 0.992$ | $k_4$ | $-7.94\times10^{-6}$ | $3.67\times10^{-6}$ | -2.16 | 7.40 |
| $CFL\ (t) = k_1(1 - e^{-k_2 t}) + k_3 t^{1/2}$ | $k_1$ | $6.48\times10^{-4}$ | $6.25\times10^{-5}$ | 10.37 | *** |
| | $k_2$ | $4.27\times10^{-1}$ | $8.20\times10^{-2}$ | 5.20 | ** |
| $r^2_{adjusted} = 0.988$ | $k_3$ | $6.20\times10^{-5}$ | $9.53\times10^{-6}$ | 6.50 | *** |
| Probability: *** < 0.1%; ** 0.1 – 1%, * 1-5% | | | | | |

**Table 6.** Coefficients from the regression analysis of CFL data for Sr-doped WBC-O paste.

| Model | | Value | Standard Error | t-Value | Prob > \|t\| (%) |
|---|---|---|---|---|---|
| $CFL\ (t) = k_1(1 - e^{-k_2 t}) + k_3 t^{1/2} + k_4 t$ | $k_1$ | $3.94\times10^{-4}$ | $1.09\times10^{-4}$ | 3.61 | * |
| | $k_2$ | $4.04\times10^{-1}$ | $0.91\times10^{-1}$ | 4.41 | ** |
| | $k_3$ | $1.31\times10^{-4}$ | $4.01\times10^{-5}$ | 3.27 | * |
| $r^2_{adjusted} = 0.991$ | $k_4$ | $-7.29\times10^{-6}$ | $3.22\times10^{-6}$ | -2.27 | 6.4 |
| $CFL\ (t) = k_1(1 - e^{-k_2 t}) + k_3 t^{1/2}$ | $k_1$ | $6.26\times10^{-4}$ | $6.01\times10^{-5}$ | 10.40 | *** |
| | $k_2$ | $3.69\times10^{-1}$ | $0.66\times10^{-1}$ | 5.59 | *** |
| $r^2_{adjusted} = 0.987$ | $k_3$ | $4.09\times10^{-5}$ | $8.89\times10^{-6}$ | 4.60 | ** |
| Probability: *** < 0.1%; ** 0.1 – 1%, * 1-5% | | | | | |

The apparent diffusion coefficient $D_a$ was derived from constant $k_3$ (Eq. 9) [57].

$$D_a = \pi \left(\frac{k_3 V}{2 S}\right)^2 \quad \text{(Eq.9)}$$

where $S/V$ is the geometrical surface area-to-volume ratio of the specimen.

The WBC-O paste sample exhibited a lower $D_a$ value ($(2.1\pm1.2)\times10^{-15}$ cm²·s⁻¹) compared to WBC-C ($(4.8 \pm 1.6)\times10^{-15}$ cm²·s⁻¹) [24], indicating enhanced Sr retention in the optimized formulation. The improved performance is likely related to differences in the mineralogical assemblages of the two cement pastes, which result in distinct microstructural properties. As reported by Laniesse *et al.* [18], increasing the initial aluminum concentration in the mixing solution from 1.6 mol.L$^{-1}$ in WBC-C to 2.5 mol.L$^{-1}$ in WBC-O produces a denser matrix with finer mesoporosity. This refined microstructure slows down diffusion of Sr, thereby improving its retention in WBC-O.

Both WBC-C and WBC-O exhibited apparent diffusion coefficients at least three orders of magnitude smaller than those reported for Portland cement-based materials, which typically range from $10^{-8}$ to $10^{-12}$ cm².s$^{-1}$, depending on the matrix formulation, testing protocol, and strontium concentration [56,59–61] (**Figure 11**). The Sr retention performance of the WBC pastes was comparable to those of calcium aluminate cement modified with sodium polyphosphate [62] and fly ash-based geopolymers [56]. The best retention, however, was reported for a magnesium potassium phosphate-based matrix [63].

According to ANSI specification, the leachability index (*LI*), defined by Eq. 10, can be used to evaluate the efficiency of radionuclide immobilization in the matrix.

 doi:10.20944/preprints202602.0348.v1



$$LI = log\left(\frac{\beta}{D_a}\right) \quad \text{(Eq. 10)}$$

where $\beta$ is a reference constant equal to 1 $cm^2.s^{-1}$.

The calculated *LI* values for the WBC pastes (*LI* = 14.3 ± 0.2 for WBC-C and *LI* = 14.7 ± 0.2 for WBC-O) largely exceeded the minimum threshold (*LI* = 6) recommended by the US Nuclear Regulatory Commission for radioactive waste disposal.

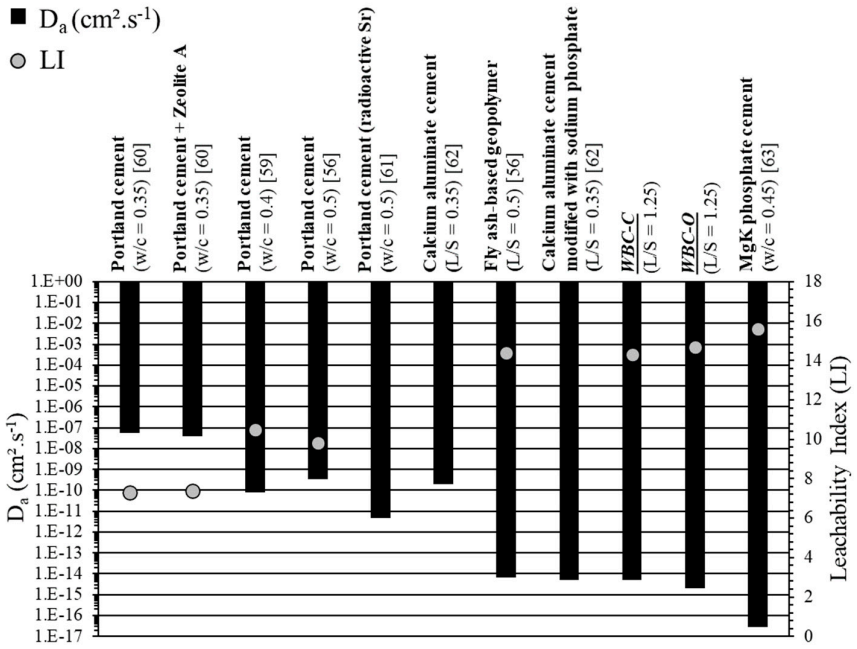


**Figure 11.** Comparison of $D_a$ values and LI of strontium reported for different materials.

## 4. Conclusion

This study evaluated the potential of Wollastonite-based Brushite Cements (WBCs) for the conditioning of low- or intermediate-level radioactive wastes contaminated with strontium-90. Two formulations were investigated: a commercial reference (WBC-C) and an optimized binder (WBC-O). After 28 days of curing under endogenous conditions, both pastes primarily consisted of amorphous phases, including hydrated silica and an aluminophosphate phase, along with crystalline brushite, residual wollastonite, and quartz.

The stability of WBC-C paste was first investigated under γ-irradiation. Up to a cumulative dose of 1 MGy, irradiation mainly induced water radiolysis, with dihydrogen production rates comparable to those reported for Portland cement-based and geopolymer matrices. Complementary experiments on brushite, the main crystalline hydrate in WBC paste, confirmed its structural stability up to 5 MGy and indicated a radiolytic yield of $H_2$ close to that obtained for portlandite ($Ca(OH)_2$), brucite ($Mg(OH)_2$) and calcium monocarboaluminate ($Ca_4Al_2(CO_3)(OH)_{12}.5H_2O$).

The influence of paste mineralogy on Sr retention was also explored. WBC-O, formulated with a higher initial aluminum concentration (2.5 $mol.L^{-1}$vs. 1.6 $mol.L^{-1}$ in WBC-C), showed improved performance, with a diffusion coefficient nearly half that of WBC-C. This enhancement is attributed to finer mesoporosity resulting from higher aluminum content, which slows down diffusion of strontium in the pore network. The leaching of strontium from both WBC pastes was well described using the semi-empirical model of Côté and Constable [57]. Two dominant mechanisms were pointed out: surface wash-off (early stage) and diffusion (later age).

Overall, these results suggest that WBCs may represent a promising option for the immobilization of Sr-containing radioactive waste. Future research should consider assessing their

 doi:10.20944/preprints202602.0348.v1



long-term leaching performance under repository-relevant alkaline conditions, as concrete in repository environments may generate high-pH plumes upon resaturation, and further elucidating the mechanisms controlling strontium retention within WBC matrices.

**Author Contributions:** Conceptualization, Céline Cau Dit Coumes, Yves Barré, Marie Noëlle de Noirfontaine and Mireille Courtial; Data curation, Jihane Jdaini; Formal analysis, Jihane Jdaini, Céline Cau Dit Coumes and Marie Noëlle de Noirfontaine; Funding acquisition, Céline Cau Dit Coumes and Marie Noëlle de Noirfontaine; Investigation, Jihane Jdaini, Céline Cau Dit Coumes and Marie Noëlle de Noirfontaine; Methodology, Jihane Jdaini, Céline Cau Dit Coumes, Yves Barré, Marie Noëlle de Noirfontaine and Mireille Courtial; Supervision, Céline Cau Dit Coumes, Yves Barré, Marie Noëlle de Noirfontaine and Mireille Courtial; Validation, Céline Cau Dit Coumes, Yves Barré, Marie Noëlle de Noirfontaine and Mireille Courtial; Writing – original draft, Jihane Jdaini, Céline Cau Dit Coumes and Marie Noëlle de Noirfontaine; Writing – review & editing, Céline Cau Dit Coumes, Yves Barré, Marie Noëlle de Noirfontaine and Mireille Courtial.

**Data Availability:** Data will be made available on request.

**Funding:** This research did not receive any specific grant from funding agencies in the public, commercial, or not-for-profit sectors.

**Declaration of Competing Interest:** The authors declare that they have no known competing financial interests or personal relationships that could have appeared to influence the work reported in this paper.

**Acknowledgments:** The authors would like to thank the support of the X-ray crystallography facility, DIFFRAX, in Ecole Polytechnique, Institut Polytechnique de Paris.

## References

1. Y. Barré, L. Schrive, C. Lepeytre, A. Hertz, A. Grandjean, and V. Blet, Decontamination of aqueous effluents, in *Clean-up and Dismantling of Nuclear Facilities*, M. Lecomte, Ed., Paris: Editions du Moniteur, 2018, 99–106.
2. M. I. Ojovan, W. E. Lee, and S. N. Kalmykov, Immobilisation of radioactive waste in cement, in *An introduction to Nuclear Waste Immobilization (3rd edition)*, Elsevier, Ed., Amsterdam, 2019, 271–303, doi: 10.1016/B978-0-08-102702-8.00017-0.
3. M. Atkins and F. P. Glasser, Application of Portland cement-based materials to radioactive waste immobilization, Waste Management, vol. 12, 105–131, 1992, doi: 10.1016/0956-053X(92)90044-J.
4. N. B. Milestone, Reactions in cement encapsulated nuclear wastes: Need for toolbox of different cement types, Advances in Applied Ceramics, vol. 105, 13–20, 2006, doi: 10.1179/174367606X81678.
5. N. D. M. Evans, Binding mechanisms of radionuclides to cement, Cement and Concrete Research, vol. 38, 543–553, 2008, doi: 10.1016/j.cemconres.2007.11.004.
6. J. Tits, E. Wieland, C. J. Müller, C. Landesman, and M. H. Bradbury, Strontium binding by calcium silicate hydrates, Journal of Colloid and Interface Science, vol. 300, 78–87, 2006, doi: 10.1016/j.jcis.2006.03.043.
7. L. Wang, M. Ochs, D. Mallants, L. Vielle-Petit, E. Martens, D. Jacques, P. De Cannière, J. A. Berry, and B. Leterme, A new radionuclide sorption database for benchmark cement accounting for geochemical evolution of cement, in *Cement-Based Materials for Nuclear Waste Storage*, F. Bart, C. Cau Dit Coumes, F. Frizon, and S. Lorente, Eds., Springer, 2013. doi: 10.1007/978-1-4614-3445-0_10.
8. K. C. Stamoulis, P. A. Assimakopoulos, K. G. Ioannides, E. Johnson, and P. N. Soucacos, Strontium-90 concentration measurements in human bones and teeth in Greece, The Science of the Total Environment, vol. 229, 165–182, 1999, doi: 10.1016/S0048-9697(99)00052-2.
9. S. P. Nielsen, The biological role of strontium, Bone, vol. 35, 583–588, 2004, doi: 10.1016/j.bone.2004.04.026.
10. K. Ohura, M. Bohner, P. Hardouin, J. Lemaître, G. Pasquier, and B. Flautre, Resorption of, and bone formation from, new beta-tricalcium phosphate-monocalcium phosphate cements: an in vivo study, Journal of Biomedical Materials Research, vol. 30, 193–200, 1996, doi: 10.1002/(SICI)1097-4636(199602)30:2<193::AID-JBM9>3.0.CO;2-M.

 doi:10.20944/preprints202602.0348.v1




11. B. R. Constantz, B. M. Barr, I. C. Ison, M. T. Fulmer, J. Baker, L. A. McKinney, S. B. Goodman, S. Gunasekaren, D. C. Delaney, J. Ross, and R. D. Poser, Histological, chemical, and crystallographic analysis of four calcium phosphate cements in different rabbit osseous sites, Journal of Biomedical Materials Research, vol. 43, 451–461, 1998, doi: 10.1002/(SICI)1097-4636(199824)43:4<451::AID-JBM13>3.0.CO;2-Q.
12. L. M. Grover, J. C. Knowles, G. J. P. Fleming, and J. E. Barralet, In vitro ageing of brushite calcium phosphate cement, Biomaterials, vol. 24, 4133–4141, 2003, doi: 10.1016/S0142-9612(03)00293-X.
13. L. M. Grover, U. Gbureck, A. J. Wright, M. Tremayne, and J. E. Barralet, Biologically mediated resorption of brushite cement in vitro, Biomaterials, vol. 27, 2178–2185, 2006, doi: 10.1016/j.biomaterials.2005.11.012.
14. N. J. S. Gorst, Y. Perrie, U. Gbureck, A. L. Hutton, M. P. Hofmann, L. M. Grover, and J. E. Barralet, Effects of fibre reinforcement on the mechanical properties of brushite cement, Acta Biomaterialia, vol. 2, 95–102, 2006, doi: 10.1016/j.actbio.2005.09.001.
15. Z. Huan and J. Chang, Novel bioactive composite bone cements based on the β-tricalcium phosphate-monocalcium phosphate monohydrate composite cement system, Acta Biomaterialia, vol. 5, 1253–1264, 2009, doi: 10.1016/j.actbio.2008.10.006.
16. J. Aberg, H. Brisby, H. B. Henriksson, A. Lindahl, P. Thomsen, and H. Engqvist, Premixed acidic calcium phosphate cement: Characterization of strength and microstructure, Journal of Biomedical Materials Research - Part B Applied Biomaterials, vol. 93, 436–441, 2010, doi: 10.1002/jbm.b.31600.
17. P. Laniesse, C. Cau Dit Coumes, A. Poulesquen, A. Bourchy, A. Mesbah, G. Le Saout, and P. Gaveau, Setting and hardening process of a wollastonite-based brushite cement, Cement and Concrete Research, vol. 106, 65–76, 2018, doi: 10.1016/j.cemconres.2018.01.019.
18. P. Laniesse, C. Cau Dit Coumes, G. Le Saout, and A. Mesbah, Understanding the setting and hardening process of wollastonite-based brushite cement. Part 2: Influence of the boron and aluminum concentrations in the mixing solution, Cement and Concrete Research, vol. 140, 106288, 2021, doi: 10.1016/j.cemconres.2020.106288.
19. C. E. Semler, Quick-setting wollastonite phosphate cement, American Ceramic Society Bulletin, vol. 55, 983–988, 1976.
20. M. H. Alkhraisat, C. Rueda, and E. López Cabarcos, Strontium ions substitution in brushite crystals: the role of strontium chloride, Journal of Functional Biomaterials, vol. 2, 31–38, 2011, doi: 10.3390/jfb2020031.
21. S. Pina, S. I. Vieira, P. Rego, P. M. C. Torres, O. A. B. da Cruz e Silva, E. F. da Cruz e Silva, and J. M. F. Ferreira, Biological responses of brushite-forming Zn-and ZnSr-substituted beta-tricalcium phosphate bone cements, European Cells & Materials, vol. 20, 162–177, 2010, doi: 10.22203/eCM.v020a14.
22. E. Boanini, M. Gazzano, and A. Bigi, Ionic substitutions in calcium phosphates synthesized at low temperature, Acta Biomaterialia, vol. 6, 1882–1894, 2010, doi: 10.1016/j.actbio.2009.12.041.
23. K. Hurle, J. M. Oliveira, R. L. Reis, S. Pina, and F. Goetz-Neunhoeffer, Ion-doped brushite cements for bone regeneration, Acta Biomaterialia, vol. 123, 51–71, 2021, doi: 10.1016/j.actbio.2021.01.004.
24. J. Jdaini, C. Cau Dit Coumes, Y. Barré, M-N. de Noirfontaine, M. Courtial, E. Garcia-Caurel, F. Dunstetter, D. Gorse-Pomonti, Strontium release from wollastonite-based brushite cement paste under semi-dynamic leaching conditions, Proc. NUWCEM 2022 (International Symposium on Cement-Based Materials for Nuclear Wastes), Avignon, France, 2022.
25. ANSI/ANS-16.1–2003 (R2017), Measurement of the leachability of solidified low-level radioactive wastes by a short-term test procedure, American National Standards Institute, Washington, DC, USA, 2017.
26. N. E. Bibler, Radiolytic gas production from concrete containing Savannah River Plant Waste, Savanah River Laboratory, Report (DP-1464), 1978, doi: 10.2172/5150618.
27. P. Bouniol and E. Bjergbakke, A comprehensive model to describe radiolytic processes in cement medium, Journal of Nuclear Materials, vol. 372, 1–15, 2008, doi: 10.1016/j.jnucmat.2006.10.004.
28. T. M. Rosseel, I. Maruyama, Y. Le Pape, O. Kontani, A. B. Giorla, I. Remec, J. J. Wall, M. Sircar, C. Andrade, and M. Ordonez, Review of the current state of knowledge on the effects of radiation on concrete, Journal of Advanced Concrete Technology, vol. 14, 368–383, 2016, doi: 10.3151/jact.14.368.
29. D. Chartier, J. Sanchez-Canet, L. Bessette, S. Esnouf, and J.-P. Renault, Influence of formulation parameters of cement based materials towards gas production under gamma irradiation, Journal of Nuclear Materials, vol. 511, 183–190, 2018, doi: 10.1016/j.jnucmat.2018.09.024.

 doi:10.20944/preprints202602.0348.v1




30. L. Acher, M.-N. de Noirfontaine, D. Chartier, D. Gorse-Pomonti, M. Courtial, S. Tusseau-Nenez, O. Cavani, J. Haas, A. Dannoux-Papin, and F. Dunstetter, $H_2$ production under gamma irradiation of a calcium aluminate cement: An experimental study on both cement pastes and its stable hydrates, Radiation Physics and Chemistry, vol. 189, 109689, 2021, doi: 10.1016/j.radphyschem.2021.109689.
31. C. J. Kertesz, P. R. Chenavas, and L. Auffret, Conditionnement de cendres d'incinérateur alpha et bêta gamma, obtenues par incinération des déchets radioactifs, par enrobage, dans différentes matrices, Commission européenne, Sciences et techniques nucléaires, Report EUR 14365 FR (in French), 1993.
32. C. Madic and G. Koehly, Comportement à long terme des matrices d'enrobage contaminées en émetteurs alpha ; Etude du phénomène de rupture d'éprouvettes constituées de liants hydrauliques contaminés en plutonium 238 et curium 244 au cours de leur lixiviation, DGR, vol.134, Report C.E.A (in French), 1986.
33. M.-N. de Noirfontaine, E. Garcia-Caurel, D. Funes-Hernando, M. Courtial, S. Tusseau-Nenez, O. Cavani, J. Jdaini, C. Cau Dit Coumes, F. Dunstetter, and D. Gorse-Pomonti, Amorphization of a proposed sorbent of strontium, brushite, $CaHPO_4.2H_2O$, studied by X-ray diffraction and Raman spectroscopy, Journal of Nuclear Materials, vol. 545, 152751, 2021, doi: 10.1016/j.jnucmat.2020.152751.
34. D. Chartier, J. Sanchez-Canet, P. Antonucci, S. Esnouf, J.-P. Renault, O. Farcy, D. Lambertin, S. Parraud, H. Lamotte, and C. Cau Dit Coumes, Behaviour of magnesium phosphate cement-based materials under gamma and alpha irradiation, Journal of Nuclear Materials, vol. 541, 152411, 2020, doi: 10.1016/j.jnucmat.2020.152411.
35. T. Herin, T. Charpentier, P. Bouniol, and S. Le Caër, Behavior of portlandite upon exposure to ionizing radiation: evidence of delayed $H_2$ production, The Journal of Physical Chemistry C, vol. 127, 20245–20254, 2023, doi: 10.1021/acs.jpcc.3c05012.
36. F. Frizon and C. Galle, Experimental investigations of diffusive and convective transport of inert gas through cement pastes, Journal of Porous Media, vol. 12, 221–237, 2009, doi: 10.1615/JPorMedia.v12.i3.30.
37. R. Snellings, J. Chwast, Ö. Cizer, N. De Belie, Y. Dhandapani, P. Durdzinski, J. Elsen, J. Haufe, D. Hooton, C. Patapy, M. Santhanam, K. Scrivener, D. Snoeck, L. Steger, S. Tongbo, A. Vollpracht, F. Winnefeld, and B. Lothenbach, RILEM TC-238 SCM recommendation on hydration stoppage by solvent exchange for the study of hydrate assemblages, Materials and Structures, vol. 51, 172, 2018, doi: 10.1617/s11527-018-1298-5.
38. R. L. Frost and S. J. Palmer, Thermal stability of the 'cave' mineral brushite $CaHPO_4{\cdot}2H_2O$ - Mechanism of formation and decomposition, Thermochimica Acta, vol. 521, 14–17, 2011, doi: 10.1016/j.tca.2011.03.035.
39. R. J. Angel, Structural variation in wollastonite and bustamite, Mineralogical Magazine, vol. 49, 37–48, 1985, doi: 10.1180/minmag.1985.049.350.05.
40. C. Frontera and J. Rodríguez-Carvajal, FullProf as a new tool for flipping ratio analysis, Physica B: Condensed Matter, vol. 335, 219–222, 2003, doi: 10.1016/S0921-4526(03)00241-2.
41. P. F. Schofield, K. S. Knight, J. A. M. van der Houwen, and E. Valsami-Jones, The role of hydrogen bonding in the thermal expansion and dehydration of brushite, di-calcium phosphate dihydrate, Physics and Chemistry of Minerals, vol. 31, 606–624, 2004, doi: 10.1007/s00269-004-0419-6.
42. Y. Ohashi, Polysynthetically-twinned structures of enstatite and wollastonite, Physics and Chemistry of Minerals, vol. 10, 217–229, 1984, doi: 10.1007/BF00309314.
43. S. M. Antao, I. Hassan, J. Wang, P. L. Lee, and B. H. Toby, State-of-the-art high-resolution powder X-ray diffraction (HRPXRD) illustrated with Rietveld structure refinement of quartz, sodalite, tremolite, and meionite, The Canadian Mineralogist, vol. 46, 1501–1509, 2008, doi: 10.3749/canmin.46.5.1501.
44. W. A. Dollase, Correction of intensities of preferred orientation in powder diffractometry: application of the March model, Journal of Applied Crystallography, vol. 19, 267–272, 1986, doi: 10.1107/S0021889886089458.
45. M. Landín, R. C. Rowe, and P. York, Structural changes during the dehydration of dicalcium phosphate dihydrate, European Journal of Pharmaceutical Sciences, vol. 2, 245–252, 1994, doi: 10.1016/0928-0987(94)90029-9.
46. J. Jdaini, Potential of brushite cement for treating and conditioning radioactive waste contaminated with strontium, PhD report (in French), Montpellier University, France, 2022.
47. P. Laniesse, Wollastonite-based brushite cements: reactivity, properties, and application to the treatment of strontium-contaminated aqueous wastestreams, PhD report (in French), Montpellier University, France, 2019.

 doi:10.20944/preprints202602.0348.v1




48. E. Huseynov, DTA and TG analysis of nano $SiO_2$ - $H_2O$ systems, The Journal of the International Association of Physics Students, 2013.
49. F. Chupin, Characterisation of irradiation effects on geopolymers, PhD report (in French), Pierre and Marie Curie University, France, 2015.
50. H. J. Möckel and R. H. Köster, Gas formation during the gamma radiolysis of cemented low- and intermediate-level waste products, Nuclear Technology, vol. 59, 494–497, 1982, doi: 10.13182/NT82-A33007.
51. B. Pastina, J.A. LaVerne, S.M. Pimblott, Dependence of molecular hydrogen formation in water on scavengers of the precursor to the hydrated electron, The Journal of Physical Chemistry A, vol. 103, 5841-5846 1999, doi:10.1021/jp991222q.
52. C. Yin, A. Dannoux-Papin, J. Haas, and J.-P. Renault, Influence of calcium to silica ratio on $H_2$ gas production in calcium silicate hydrate, Radiation Physics and Chemistry, vol. 162, 66–71, 2019, doi: 10.1016/j.radphyschem.2019.04.035.
53. J. A. LaVerne and L. Tandon, $H_2$ and $Cl_2$ production in the radiolysis of calcium and magnesium chlorides and hydroxides, The Journal of Physical Chemistry A, vol. 109, 2861–2865, 2005, doi: 10.1021/jp044166o.
54. L. Acher, Investigation of the behaviour of cement matrices and their hydrates under $\gamma$ and electron irradiation, PhD report (in French), Paris Saclay University, France, 2017.
55. M.-N. de Noirfontaine, M. Courtial, A. Alessi, S. Tusseau-Nenez, E. Garcia-Caurel, O. Cavani, C. Cau Dit Coumes, and D. Gorse-Pomonti, Stability under electron irradiation of some layered hydrated minerals, Journal of Solid State Chemistry, vol. 340, 125033, 2024, doi: 10.1016/j.jssc.2024.125033.
56. J. G. Jang, S. M. Park, and H. K. Lee, Physical barrier effect of geopolymeric waste form on diffusivity of cesium and strontium, Journal of Hazardous Materials, vol. 318, 339–346, 2016, doi: 10.1016/j.jhazmat.2016.07.003.
57. P. L. Côtê, T. W. Constable, and A. Moreira, An evaluation of cement-based waste forms using the results of approximately two years of dynamic leaching, Nuclear and Chemical Waste Management, vol. 7, 129–139, 1987, doi: 10.1016/0191-815X(87)90007-6.
58. C. Pescatore and A. J. Machiels, Effect of surfaces on glass waste form leaching, Journal of Non-Crystalline Solids, vol. 49, 379–388, 1982, doi: 10.1016/0022-3093(82)90133-8.
59. J.-Y. Goo, B.-J. Kim, M. Kang, J. Jeong, H. Y. Jo, and J.-S. Kwon, Leaching behavior of cesium, strontium, cobalt, and europium from immobilized cement matrix, Applied Sciences, vol. 11, 8418, 2021, doi: 10.3390/app11188418.
60. A. M. El-Kamash, M. R. El-Naggar, and M. I. El-Dessouky, Immobilization of cesium and strontium radionuclides in zeolite-cement blends, Journal of Hazardous Materials, vol. 136, 310–316, 2006, doi: 10.1016/j.jhazmat.2005.12.020.
61. H. Matsuzuru and A. Ito, Leaching behaviour of strontium-90 in cement composites, Annals of Nuclear Energy, vol. 4, 465–470, 1977, doi: 10.1016/0306-4549(77)90020-2.
62. K. Irisawa, M. Namiki, T. Taniguchi, I. Garcia-Lodeiro and H. Kinoshita, Solidification and stabilization of strontium and chloride ions in thermally treated calcium aluminate cement modified with or without sodium polyphosphate, Cement and Concrete Research, vol. 156, 106758, 2022, doi: 10.1016/j.cemconres.2022.106758.
63. J.-Y. Pyo, W. Um, and J. Heo, Magnesium potassium phosphate cements to immobilize radioactive concrete wastes generated by decommissioning of nuclear power plants, Nuclear Engineering and Technology, vol. 53, 2261–2267, 2021, doi: 10.1016/j.net.2021.01.005.